NANO LETTERS

pubs.acs.org/NanoLett Letter

Tunable Tribovoltaic Effect via Metal−Insulator Transition

Ruizhe Yang, Zihao He, Shiquan Lin, Wenjie Dou, Zhong Lin Wang, Haiyan Wang, and Jun Liu*

Cite This: *Nano Lett.* 2022, 22, 9084−9091 Read Online

ACCESS | Metrics & More | Article Recommendations | Supporting Information

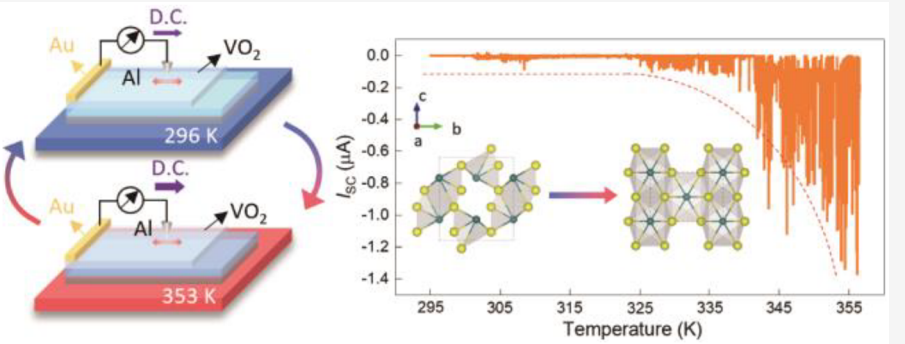

ABSTRACT: Tribovoltaic direct-current (DC) nanogenerator made of dynamic semiconductor heterojunction is emerging as a promising mechanical energy harvesting technology. However, fundamental understanding of the mechano-electronic carrier excitation and transport at dynamic semiconductor interfaces remains to be investigated. Here, we demonstrated for the first time, that tribovoltaic DC effect can be tuned with metal-insulator transition (MIT). In a representative MIT material (vanadium dioxide, VO_2), we found that the short-circuit current (I_{SC}) can be enhanced by >20 times when the material is transformed from insulating to metallic state upon static or dynamic heating, while the open-circuit voltage (V_{OC}) turns out to be unaffected. Such phenomenon may be understood by the Hubbard model for Mott insulator: orders' magnitude increase in conductivity is induced when the nearest hopping changes dramatically and overcomes the Coulomb repulsion, while the Coulomb repulsion giving rise to the quasi-particle excitation energy remains relatively stable.

KEYWORDS: *energy harvesting, tribovoltaic effect, nanogenerators, metal−insulator transition*

The new era of Internet of things (IoTs) shows increasing demand for sustainable energy solutions for self-powered miniaturized electronics for various applications such as distributed sensor networks, wearable electronics, and implantable devices.[1−3] Dynamic semiconductor heterojunction based tribovoltaic DC generators have emerged as a new strategy for high-DC-energy harvesting,[4] with the strength of remarkable advantages of high current density (10−100 A m^{-2}, 3−4 orders higher than that of traditional approaches based on the displacement of a dielectric layer).[4−8] The tribovoltaic effect is a process in which electron−hole pairs are excited during contact due to the energy released by the newly formed bonds, which can be named "bindington". The electron−hole pairs are further driven by the built-in electric field to move from one side to the other side at the interfaces, generating a direct current.[7,9−12] The carrier excitation is believed to be associated with a quantum dynamic process involving electron−phonon coupling.[13−15] Meanwhile, the existence of an interfacial layer, adsorption, image charges, surface/geometry-sensitive electromechanical coupling (e.g., piezoelectricity or flexoelectricity) at physical contacts, and nonequilibrium drift-diffusion current may also contribute to the overall voltage output.[16−21] It is experimentally known that the DC density is associated with voltage output as the driving force, as well as series resistance as the barrier for current flow.[4] As predicted by traditional band theory, metal/metal dynamic contacts exhibit a negligible tribovoltaic potential difference (or voltage output) due to the instantaneous alignment of Fermi levels in a few microseconds and ultrafast electron−hole pair recombination, which has been supported by experimental observations.[14,22−24]

However, this hypothesis may be less obvious in a strongly correlated system: for instance, a metal−insulator transition (MIT) material. During the MIT, the material undergoes an electronic phase transition from a metallic (M) state to an insulating (I) state by various external stimuli (i.e., increasing temperature, pressure, or electric field).[25] Based on the specific changes in the electronic and crystallographic structures, a

Received: September 6, 2022
Revised: November 2, 2022
Published: November 7, 2022

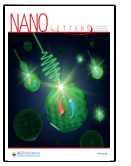

https://doi.org/10.1021/acs.nanolett.2c03481
Nano Lett. 2022, 22, 9084−9091

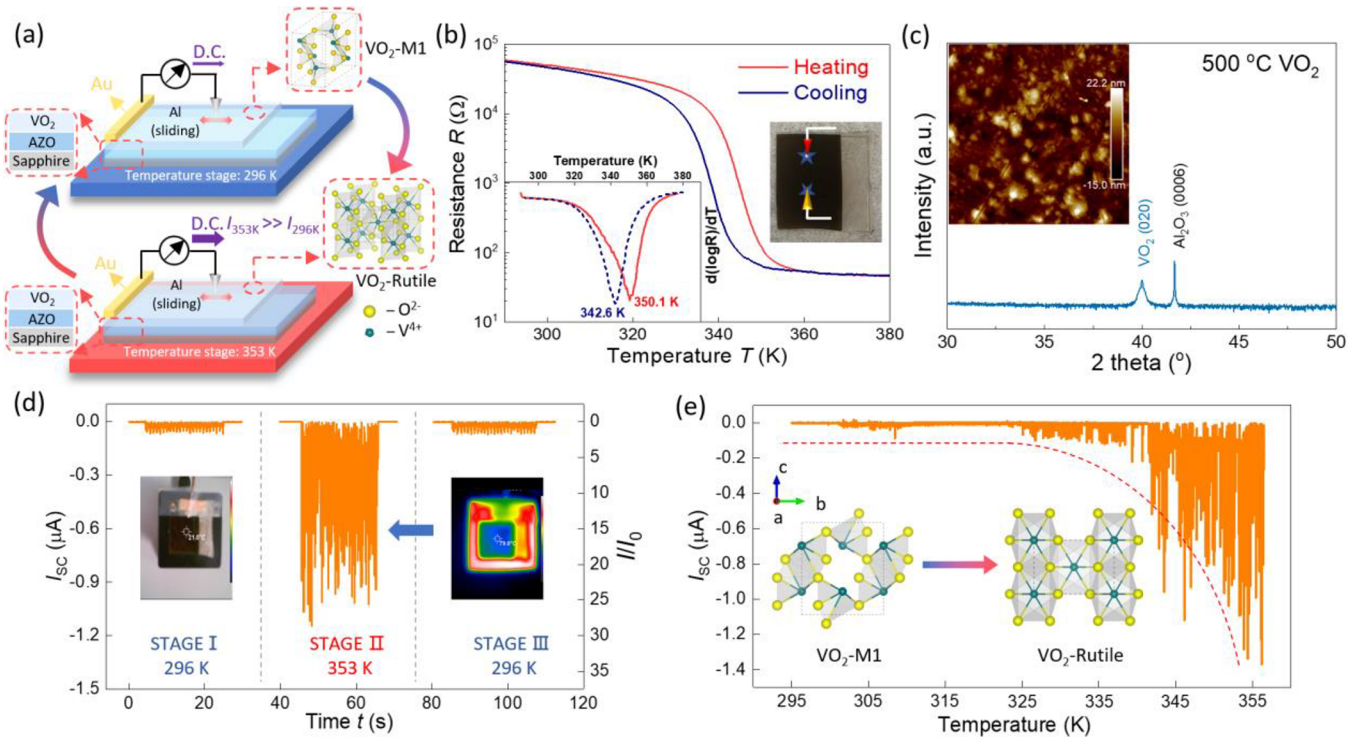

Figure 1. (a) Schematic illustration of Al/VO_2 sliding contacts. (b) Resistance−temperature plots of the as-synthesized VO_2 thin film. The T_c value of VO_2 is around 345 K. Inset: resistivity change rate of VO_2 films. (c) XRD θ−2θ spectra of VO_2 thin films on c-cut sapphire substrates. Inset: AFM topological image of the VO_2 thin film. (d) Short-circuit current (I_{SC}) at stage I before heating (room temperature: ∼296 K), at stage II on heating to ∼353 K, and stage III on cooling back to room temperature (∼296 K) under 0.1 MPa pressure. Inset: thermal image at stages I and III (left) and at stage II (right). (e) Real-time I_{SC} of Al/VO_2 sliding contacts as the temperature is increased continuously under 0.1 MPa pressure. Inset: illustration of the crystal structure changing from VO_2-M1 (monoclinic) to VO_2-rutile (tetragonal).

structure-driven Peierls transition mechanism or electron-dependent mechanism may be responsible for the narrowing of the band gap and the collapse of lattice symmetry (crystal structure shifting from a monoclinic insulator to a rutile metal).[26−28] In addition, the Mott−Hubbard mechanism describes phase transitions in a large class of materials, i.e., Mott insulating materials, where a strong Coulomb repulsion between electrons in outer orbitals plays a crucial role.[29] The Mott transition process requires electrons to gain enough energy to overcome the Coulomb barrier, which can be achieved by temperature changes or by applying stress.[30] As a representative correlated electron system, the MIT transition of vanadium dioxide (VO_2)[31] can be triggered by temperature, pressure, electric field, and irradiation (photothermal) with an ultrafast phase transition (within 0.1 K) and a phase transition temperature (T_c) from an I state (monoclinic structure) to a M state (rutile structure) around 341 K.[32] Herein, for the first time, we prove that the tribovoltaic DC short-circuit current across a MIT material (VO_2) can be enhanced by orders of magnitude while a relative steady V_{OC} output is maintained upon a phase transition, which is in sharp contrast to the traditional material systems where V_{OC} and I_{SC} are usually inversely proportional to each other.

To demonstrate the tunable tribovoltaic effect on metal/VO_2 sliding contacts, as shown in Figure 1a, an aluminum (Al) metal probe (diameter ∼1 mm) was slid over a piece of VO_2 (145 nm, prepared by pulsed layer deposition (PLD))/aluminum-doped zinc oxide (AZO, 55 nm) thin film on c-cut sapphire substrates (500 μm). The sample temperature is controlled by a tunable heating stage and monitored by an infrared (IR) camera. VO_2 thin films were deposited at 773 K. The MIT properties of the VO_2 thin film were characterized by measuring the temperature-dependent electrical resistance switching during the phase transition. Figure 1b shows the electrical resistance of the VO_2 thin film as a function of increasing/decreasing temperature (under a temperature ramping rate of 5 K min^{-1}, Au probe and back electrode). The resistivity and the resistivity change rate (in units of Ω m K^{-1}) as a function of temperature are shown in Figure 1b. The transition temperature (T_c) of pure VO_2 film deposited on c-cut sapphire, which is defined as the temperature required to induce a change from an I state to an M state, shows a value (350 K) similar to those in prior work.[33,34] Figure 1c shows the X-ray diffraction (XRD) spectrum of the VO_2 thin film with a distinct diffraction peak corresponding to VO_2 (M1) (020), indicating a highly textured growth of monoclinic VO_2 along the b axis. The inset in Figure 1c shows an atomic force microscopy (AFM) topographic image of the as-prepared VO_2 thin film, where a highly uniform film surface is observed with a calculated root-mean-square surface roughness (R_q) of 4 nm. It can be seen that the thin film shows an excellent film quality, a high transition amplitude, and a sharp transition.

For a tribovoltaic DC generation with Al/VO_2 sliding contacts, the I_{SC} output under multiple temperature stages has been measured by a motor-driven testing system with a precise control of the applied force and sliding velocity (Figure 1d): stage I, at room temperature (296 K surface temperature as indicated by thermal image), where the sample is at original insulator state; stage II, on heating up to 353 K, where the sample transits into M state; stage III, on cooling to room temperature (296 K), where the sample shifts back to the I state. An I_{SC} of around 0.06 μA (corresponding current density

https://doi.org/10.1021/acs.nanolett.2c03481
Nano Lett. 2022, 22, 9084−9091

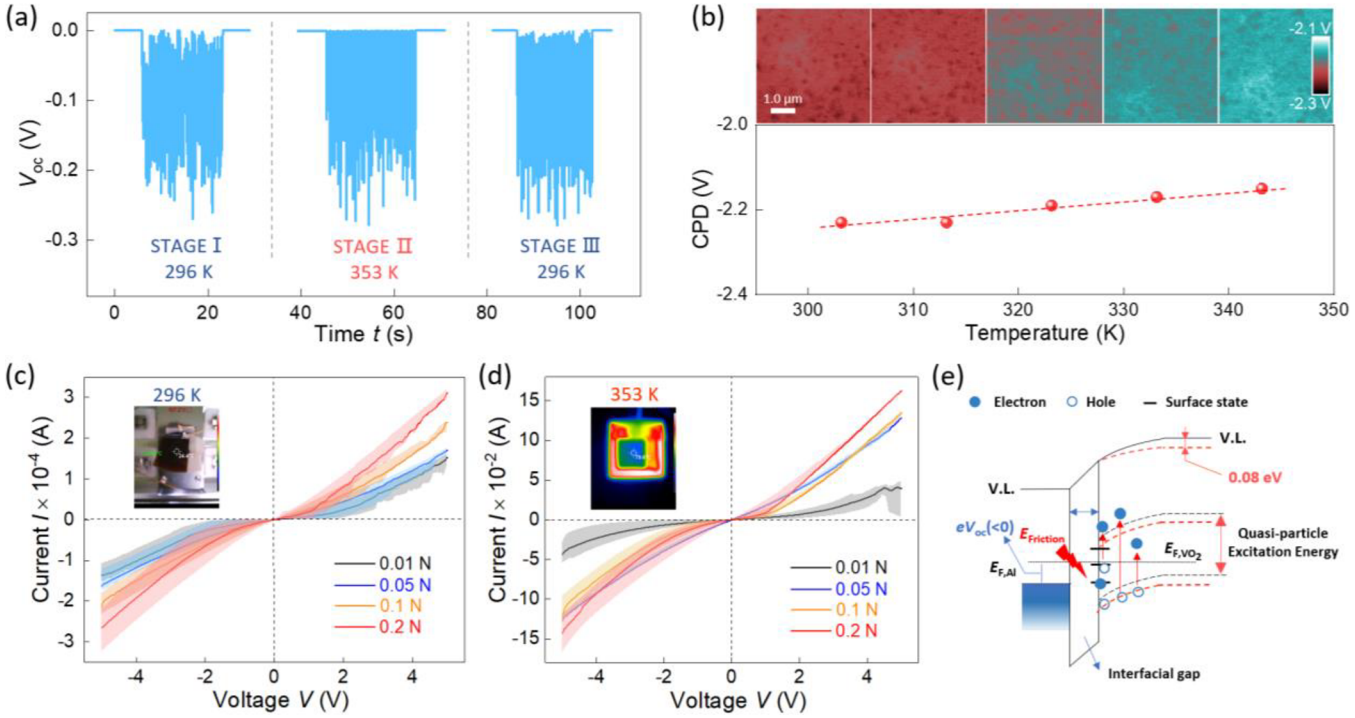

Figure 2. (a) Open-circuit current V_{OC} at stage I before heating (room temperature: 296 K), stage II on heating to 353 K, and stage III on cooling back to room temperature (296 K). (b) Averaged contact potential difference (CPD) calculated by KPFM as a function of temperature (303.15 to 343.15 K), Inset: KPFM potential mapping at 303.15, 313.15, 323.15, 333.15, and 343.15 K, respectively. Force-dependent static $I-V$ characterizations of Al/VO_2 sliding contacts at (c) room temperature (~296 K) and (d) ~353 K under 0.01, 0.05, 0.1, and 0.2 N, respectively, which displays both the Schottky contact feature and decrease in series resistance as the applied force increases. The error band area represents the standard deviation. (e) Open-circuit band diagram of Al/VO_2 sliding contacts before (I state: black band) and after (M state: red band) the phase transition of VO_2.

J_{SC} of 0.06 A m^{-2}) was observed under the insulator state, in stages I and III, whereas the I_{SC} in stage II under the M state is found to be up to 1.15 μA (corresponding current density J_{SC} of 1.15 A m^{-2}), which is an ~20 times enhancement compared to the output at room temperature. Real-time I_{SC} is also measured as a function of surface temperature ,as shown in Figure 1e. The I_{SC} increases from 0.05 to 1.41 μA as the thin-film temperature increases continuously from 296 to 356 K. Both measurements were carried out under a pressure of 0.1 MPa and a sliding speed of 15 mm s^{-1}. Such a DC output boost is in line with the orders of magnitude decrease of resistance of VO_2 upon an MIT phase transition (Figure 1c). It is noted that the order of enhancement may not exactly match with that of resistance change due to the existence of tip-plane contact resistance along with the changing bulk resistance. In order to further confirm the completion of an MIT phase transition, DC generation at higher temperature (365 K) has been measured as shown in Figure S6 in the Supporting Information. An ~23 times enhancement of DC output compared to that generated at 296 K has been observed, where the magnitude of enhancement is consistent with the measured result at 353 K.

To further investigate the driving force of the DC generation, V_{OC} measurements at stages I–III were also conducted (tested under a pressure of 0.1 MPa and a sliding speed of 15 mm s^{-1}). As shown in Figure 2a, unlike the orders of magnitude variation in I_{SC}, a consistent V_{OC} output of ~0.25 V was observed between the I state and M state. Here, it is inferred that the steady V_{OC} output is ascribed to the limited work function variation between I and M states of VO_2, as well as its special quasi-particle excitation energy structure.[35] To first investigate the work function variation, temperature-controlled Kelvin probe force microscopy (KPFM) has been carried out on the as-synthesized VO_2 thin films. The KPFM surface potential mappings shown in Figure 2b display the surface potential variation trend and high uniformity of surface potential. The average contact potential difference (CPD) only shows a slight increase of 0.08 V when the temperature climbs from 303.15 to 343.15 K, indicating a small variation in work function before and after the phase transition, which is in good agreement with previous reports.[35]

To further understand the mechanism of the DC generation effect, force-dependent static $I-V$ characterizations of I (Figure 2c: 296 K) and M states (Figure 2d: 353 K) have been conducted based on an Al/VO_2 sliding contact under pressures of 0.01, 0.05, 0.1, and 0.2 MPa, respectively. For both I and M states, it can be seen that all $I-V$ measurements display a nonlinear feature, which is an indication of Schottky contact formation with a rectifying effect.[7,18,36] Moreover, the current increases with increasing applied pressure at the interface, suggesting the contact resistance decreases as the pressure rises. Additionally, the $I-V$ characterizations of VO_2 at the I state in Figure 2c displays a value 2 orders of magnitude lower than that of VO_2 at the M state (Figure 2d) in terms of current amplitude, which can be ascribed to the much higher resistance of the VO_2 thin film before the phase transition. Notably, the Schottky feature can still be observed in the Al/M-state VO_2 contact. Furthermore, the energy band diagram in Figure 2e illustrates the Al/VO_2 contact interface with an interfacial gap under an open-circuit condition. It is proposed that

https://doi.org/10.1021/acs.nanolett.2c03481
Nano Lett. 2022, 22, 9084−9091

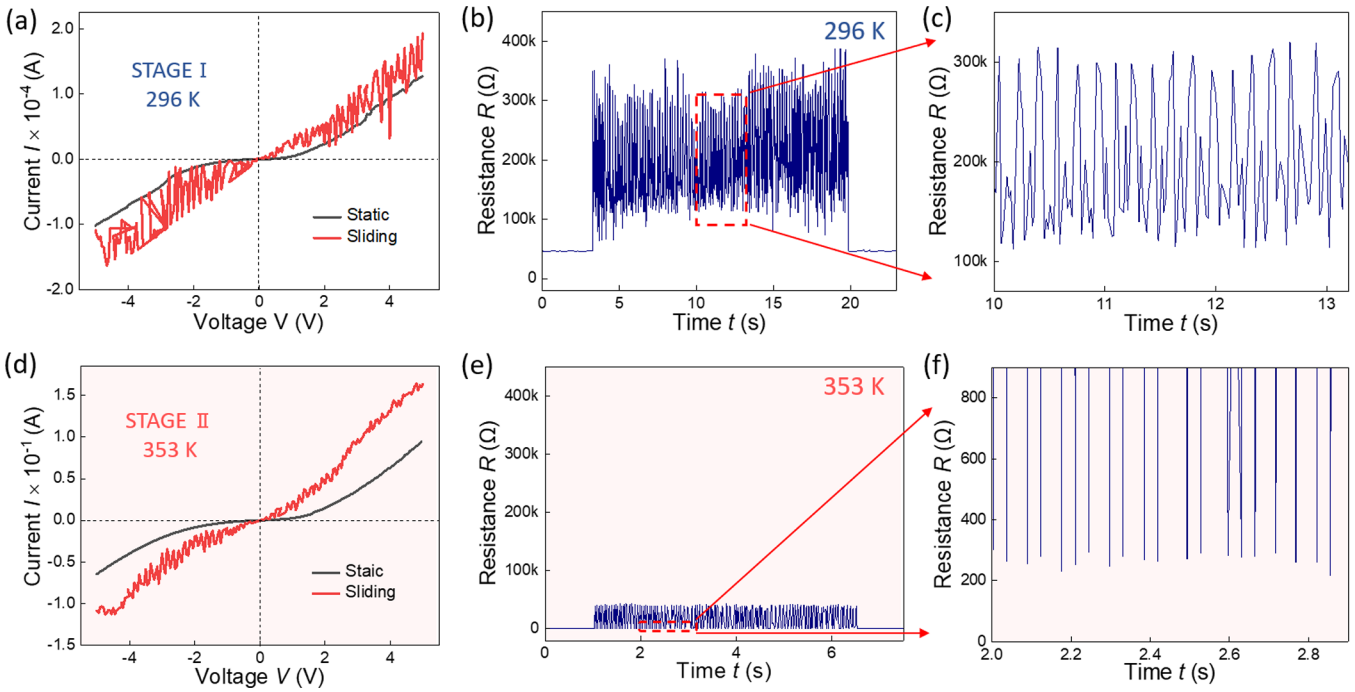

Figure 3. (a) Comparison of room-temperature $I-V$ characterization of the Al/VO_2 contact under static and sliding conditions. (pressure of 0.1 MPa, sliding speed of 15 mm s^{-1}). (b) Contact resistance fluctuation with Al/VO_2 sliding contacts at room temperature (~296 K). (c) Enlarged figure showing the detailed contact resistance profile. (d) Comparison of $I-V$ characterization of the Al/VO_2 junction under static and sliding conditions (pressure of 0.1 MPa). (e) Resistance fluctuation with Al/VO_2 sliding contacts after a phase transition (~353 K). (f) Enlarged figure showing the detailed contact resistance profile.

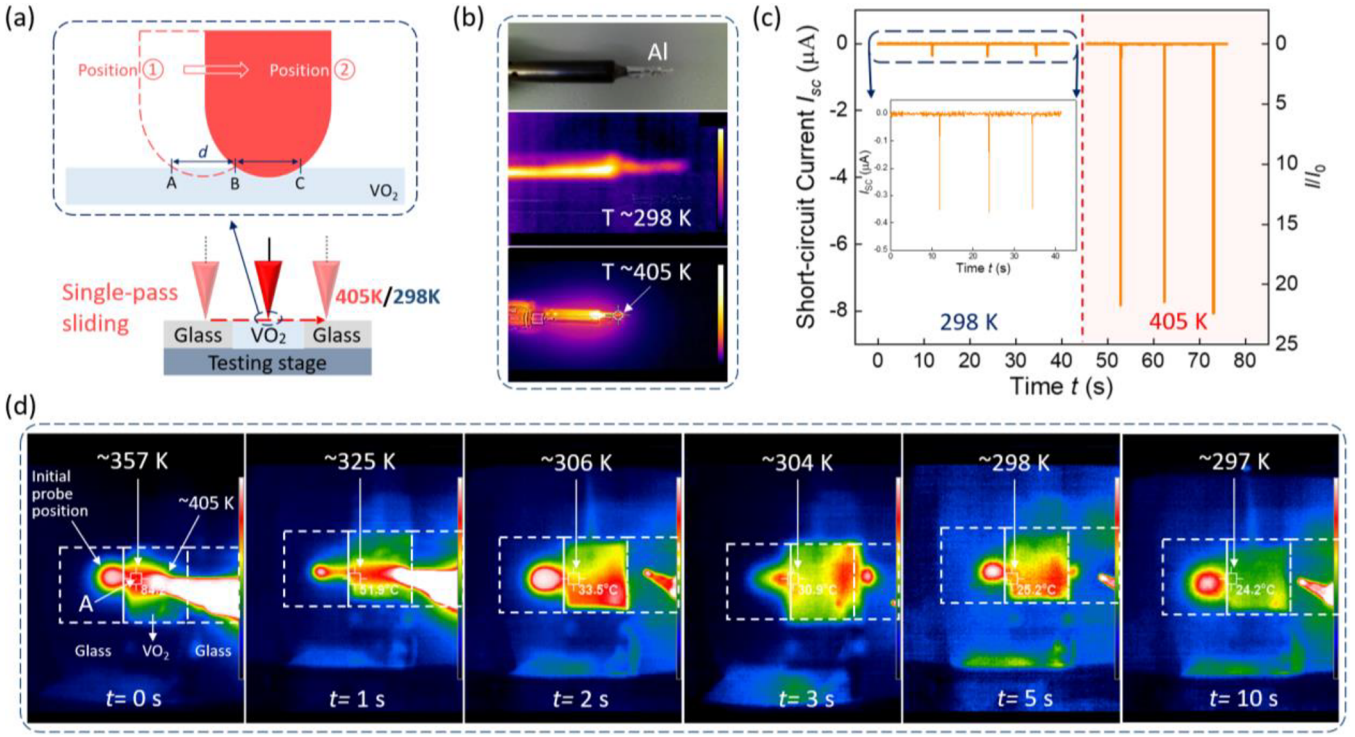

Figure 4. (a) Schematic demonstration of the tribovoltaic effect under fast a MIT transition with dynamic heating of VO_2, where the VO_2 thin film sample is positioned between two glass slides and an Al-wrapped soldering probe is employed to perform sliding at both room temperature (298 K) and high temperature (~405 K). (b) Photo image (top) and IR images (middle, room temperature, 298 K; bottom, high temperature, ~405 K) of the probe. (c) Corresponding I_{SC} measurements at room temperature and high temperature with multiple testing cycles. The time interval between each cycles is 10 s. (d) Real-time IR images with local temperature distribution throughout a single-pass sliding process, from presliding to 10 s after sliding.

https://doi.org/10.1021/acs.nanolett.2c03481
Nano Lett. 2022, 22, 9084−9091

tribovoltaic carriers are excited by the frictional energy employed at an Al/VO_2 sliding interface, transmit across the interfacial energy barrier (Schottky barrier) via direct quantum tunneling and thermionic emission/trap-assisted transport, and get oriented by the built-in electric field in the surface charged region (SCR).

Here, it should be emphasized that the band gap of a Mott insulator is different from that of a traditional semiconductor such as silicon. The electronic properties of a Mott insulator can be understood from the Hubbard model, where there is a strong Coulomb repulsion U and the nearest hopping V.[37,38] The Coulomb repulsion U gives rise to an electron−hole band gap which is directly related to V_{OC}. During the insulator−metal transition, it is believed that the change of Coulomb repulsion is limited, mainly due to the weak carrier screening effects at the sliding surface, whereas the nearest hopping V changes dramatically. When the nearest hopping V overcomes the Coulomb repulsion U, an insulator−metal transition happens.[37,38] This explanation agrees with our observation well. We do see that V_{OC} does not change much, whereas the electronic conductance changes dramatically during the insulator−metal transition. Notably, tribovoltaic DC cannot be generated in a dissimilar metal/metal sliding contact system; even the work functions of the two metals are different. This can be ascribed to the absence of an energy band gap in a metal such that any electronic excitation of electron−hole pairs will recombine instantaneously, which has been predicted by our previous quantum dynamic study on the tribovoltaic effect.[14] Meanwhile, the surface dipoles due to contact electrification of two dissimilar metals are confined on the very surface, providing no spatially distributed electric field for separating the electron−hole pairs for DC flow. However, the existence of quasi-particle excitation energy in VO_2 allows effective electronic excitation and transport of carriers for DC generation. Therefore, the Al/VO_2 (M state) sliding system cannot be regarded as equivalent to a metal/metal sliding contact.

Furthermore, Figure 3a,d shows a comparison of the $I-V$ curves between static and dynamic (under sliding; pressure 0.1 MPa and sliding speed of 15 mm s^{-1}) conditions for the I (Figure 3a: 296 K) and M states (Figure 3d: 353 K), respectively. At both the I and M states, a typical Schottky type of rectifying $I-V$ curve is measured.[7,18,36] However, when the Al probe is rubbed over the VO_2 thin film, the DC output is observed to be amplified from 0.01 to ∼197 μA for the I state (296 K) and from 0.01 to 1.6×10^5 μA for the M state (353 K) with increases in the bias voltage from 0 to 5 V. Such current magnification is due to the addition of tribovoltaic current to the signal under static conditions. Also, it is worth pointing out that, compared with the $I-V$ curves of the I state, a 3 orders of magnitude current amplitude augmentation of the M state was observed, which is also due to the resistance drop caused by the phase transition of VO_2 and is in good agreement with I_{SC} output data (Figure 1d). Furthermore, contact resistances under sliding motion for the I (Figure 3b,c: 296 K) and M states (Figure 3e,f: 353 K) were monitored and recorded, respectively. It should be noted that the contact resistance fluctuation of the M state (353 K) shown in Figure 3e (from 50 to 300 kΩ) appears to be considerably greater than that of I state (296 K) shown in Figure 3b (from 200 to 40 kΩ).

Moreover, a single-pass sliding method has been introduced to investigate the tribovoltaic effect under fast MIT. As shown in Figure 4a (bottom), an Al-wrapped soldering probe (heating capability up to 650 ± 4 K) is applied to slide over a VO_2 thin film (PLD), where the VO_2 sample is placed between two glass slides (one on each side) to eliminate a preheating issue of the VO_2 thin film prior to the sliding motion. Here, the sliding probe starts from the glass (left), slides over the VO_2 thin film, and stops on the glass (right). The duration of the probe on the sample surface, $\lambda \approx 1$ s, corresponding to a sliding velocity $v \approx 1.5$ mm s^{-1}. The middle and the bottom IR images in Figure 4b show the probe temperature under unheated (298 K) and heated (405 K), conditions, respectively. The IR images in Figure 4d record the evolution of the VO_2 film surface temperature during a representative single-pass sliding process (from $t \approx 0$ s to $t \approx 10$ s, where $t = 0$ is defined as the moment right after the probe passes point A on the VO_2 thin film as shown in Figure 4d). It can be seen that the surface temperature of VO_2 was quickly increased to >357 K while the probe was passing the surface ($t = 0$ s) and sharply dropped under 325 K when the probe was leaving point A on the surface ($t = 1$ s). The surface temperature then gradually decreases to 306, 304, and 298 K when $t = 2$, 3, and 5 s, respectively, and eventually stabilizes at room temperature (297 K) when $t = 10$ s, which indicates that the VO_2 thin film switches back to the I state.

In the meantime, short-circuit current measurements were carried out. As shown in Figure 4c, I_{SC} values of 0.38 and 8.01 μA were observed at 298 and 405 K, respectively, which correspond to a ∼21 times current output enhancement. During the measurement, each sliding was performed at a 10 s interval to ensure that there was no thermal residue and the VO_2 was transformed back to the I state. As shown in Figure 4a, the duration T is defined as the travel time of the probe on one local spot (position B in Figure 4a) of VO_2, which corresponds to the duration of the probe sliding from position 1 to position 2. d is approximately the diameter of the sliding probe (∼1.5 mm). Hence, the total duration of the probe on position B (T) is the available time window for triggering the phase transition of VO_2, which can be estimated as

$$T = \frac{d}{v} = \frac{d\lambda}{l}$$

where v is the tip velocity, d is the diameter of the sliding probe (∼1.5 mm), and l is the total length of the VO_2 thin film (∼15 mm). Accordingly, T is estimated to be <0.1 s, which is orders of magnitudes higher compared to the typical time required to trigger the phase transition of VO_2 (100 fs to nanoseconds).[39−41] Therefore, the observed DC enhancement can be ascribed to the dynamic MIT under the sliding heating probe, which is in good accordance with the results obtained under a constant sample heating condition. In addition to direct heating, we also note that a fast laser or switching electric field may also be used to activate dynamic MIT in Mott insulator systems, which is worth exploring for investigating such effects in the future.[42,43]

Furthermore, metal-dependent power outputs were measured with different contact metallic materials. Figures S5 and S6 show the I_{SC} and V_{OC} outputs of I and M states of VO_2, collected with aluminum, titanium nitride (TiN), copper, silver, iron, and gold probes. It was determined that I_{SC} shows a good accordance with the work functions of different contact metals: aluminum > TiN > copper > silver > iron > gold. In addition, an I_{SC} amplification phenomenon has been observed with all tested metallic materials under heating conditions,

https://doi.org/10.1021/acs.nanolett.2c03481
Nano Lett. 2022, 22, 9084−9091

which validates the universality of tunable tribovoltaic DC generation in metal/VO_2 sliding contacts. V_{OC} values with different metals exhibit a weak work function dependence, aluminum (−0.25 V), TiN (−0.09 V), copper (0.04 V), silver (0.04 V), iron (0.21 V), gold (0.02 V) (Figure S6), which may be associated with a surface pinning effect due to the existence of surface states.[44−46]

In order to further understand the role of a Schottky contact in the DC generation phenomenon, metal-dependent $I-V$ characterizations have been carried out (Figures S6a−f and S7). It is evident from the $I-V$ characterization with different metals (Figure S6a−f) that a Schottky contact with a rectifying effect (Al, TiN, and Fe) shows the maximum V_{OC}, whereas the ideal Ohmic contact (Cu, Ag, and Au) shows the minimum V_{OC}. Such an electronic interface feature may facilitate the directional DC power generation and conduction. These results are in good accordance with previous reports in a metal/inorganic semiconductor sliding DC generator system.[47−49]

In summary, a tribovoltaic effect induced DC energy generation via a metal/MIT material (VO_2) sliding contact has been demonstrated for the first time with a tunable and controllable output performance. Under such a phase transition from the I to the M state, a 20 times enhancement in DC current has been observed in the Al/VO_2 sliding system by modulating the contact resistance variation due to the temperature-triggered sharp MIT effect; while, in the meantime, the V_{OC} value remains at a constant output level, which not only proves that the DC current output could be tuned individually but also indicates a new phenomenon that is related to the special electronic properties of a Mott insulator. It is proposed that V_{OC} remains unaffected upon heating, since the quasi-particle excitation energy resulting from Coulomb repulsion does not change too much after the MIT phase transition. In contrast, the nearest hopping changes dramatically, overcoming the Coulomb repulsion and resulting in a significantly reduced resistance and hence an enhancement of the current output.

■ ASSOCIATED CONTENT

Supporting Information

The Supporting Information is available free of charge at https://pubs.acs.org/doi/10.1021/acs.nanolett.2c03481.

Additional experimental details, materials, and methods, temperature-dependent KPFM topological image, and metal, force, and speed-dependent electrical output measurements of the Al/VO_2 contact system (PDF)

■ AUTHOR INFORMATION

Corresponding Author

Jun Liu − *Department of Mechanical and Aerospace Engineering, University at Buffalo, The State University of New York, Buffalo, New York 14260, United States; RENEW (Research and Education in Energy, Environment and Water) Institute, University at Buffalo, The State University of New York, Buffalo, New York 14260, United States;* orcid.org/0000-0001-6951-8826; Email: jliu238@buffalo.edu

Authors

Ruizhe Yang − *Department of Mechanical and Aerospace Engineering, University at Buffalo, The State University of New York, Buffalo, New York 14260, United States*

Zihao He − *School of Electrical and Computer Engineering, Purdue University, West Lafayette, Indiana 47907-2045, United States*

Shiquan Lin − *Beijing Institute of Nanoenergy and Nanosystems, Chinese Academy of Sciences, Beijing 100083, People's Republic of China; School of Nanoscience and Technology, University of Chinese Academy of Sciences, Beijing 100049, People's Republic of China*

Wenjie Dou − *School of Science, Westlake University, Hangzhou, Zhejiang 310024, People's Republic of China; Institute of Natural Sciences, Westlake Institute for Advanced Study, Hangzhou, Zhejiang 310024, People's Republic of China;* orcid.org/0000-0001-5410-6183

Zhong Lin Wang − *Beijing Institute of Nanoenergy and Nanosystems, Chinese Academy of Sciences, Beijing 100083, People's Republic of China; School of Nanoscience and Technology, University of Chinese Academy of Sciences, Beijing 100049, People's Republic of China; School of Materials Science and Engineering, Georgia Institute of Technology, Atlanta, Georgia 30332-0245, United States;* orcid.org/0000-0002-5530-0380

Haiyan Wang − *School of Electrical and Computer Engineering, Purdue University, West Lafayette, Indiana 47907-2045, United States; School of Materials Engineering, Purdue University, West Lafayette, Indiana 47907-2045, United States;* orcid.org/0000-0002-7397-1209

Complete contact information is available at: https://pubs.acs.org/10.1021/acs.nanolett.2c03481

Author Contributions

J.L. conceived the idea of the work. R.Y. and J.L. designed and conducted the experiments. Z.H. carried out the materials synthesis and characterization. S.L. conducted the temperature-dependent KPFM study. W.D. conducted the model analysis. The manuscript was written through contributions of all authors. All authors have given approval to the final version of the manuscript.

Notes

The authors declare no competing financial interest.

■ ACKNOWLEDGMENTS

J.L. gratefully acknowledges funding support from the University at Buffalo Accelerator Funds. The authors also acknowledge the assistance from Dr. Thomas Thundat (UB) and Ms. Yaoli Zhao (UB). Z.H. and H.W. acknowledge support from the U.S. National Science Foundation (DMR-1809520) for thin film deposition and the XRD effort.

■ REFERENCES

(1) Wang, H.; Wang, J.; Yao, K.; Fu, J.; Xia, X.; Zhang, R.; Li, J.; Xu, G.; Wang, L.; Yang, J.; Lai, J.; Dai, Y.; Zhang, Z.; Li, A.; Zhu, Y.; Yu, X.; Wang, Z. L.; Zi, Y. A paradigm shift fully self-powered long-distance wireless sensing solution enabled by discharge-induced displacement current. *Sci. Adv.* **2021**, *7* (39), No. eabi6751.

(2) Dong, K.; Peng, X.; An, J.; Wang, A. C.; Luo, J.; Sun, B.; Wang, J.; Wang, Z. L. Shape adaptable and highly resilient 3D braided triboelectric nanogenerators as e-textiles for power and sensing. *Nat. Commun.* **2020**, *11* (1), 2868.

(3) Yi, J.; Dong, K.; Shen, S.; Jiang, Y.; Peng, X.; Ye, C.; Wang, Z. L. Fully Fabric-Based Triboelectric Nanogenerators as Self-Powered Human−Machine Interactive Keyboards. *Nano-Micro Lett.* **2021**, *13* (1), 103.
(4) Yang, R.; Xu, R.; Dou, W.; Benner, M.; Zhang, Q.; Liu, J. Semiconductor-based dynamic heterojunctions as an emerging strategy for high direct-current mechanical energy harvesting. *Nano Energy* **2021**, *83*, 105849.
(5) Liu, J.; Zhang, Y.; Chen, J.; Bao, R.; Jiang, K.; Khan, F.; Goswami, A.; Li, Z.; Liu, F.; Feng, K.; Luo, J.; Thundat, T. Separation and Quantum Tunneling of Photo-generated Carriers Using a Tribo-Induced Field. *Matter* **2019**, *1* (3), 650−660.
(6) Wang, Z. L. Triboelectric Nanogenerators as New Energy Technology for Self-Powered Systems and as Active Mechanical and Chemical Sensors. *ACS Nano* **2013**, *7* (11), 9533−9557.
(7) Liu, J.; Goswami, A.; Jiang, K.; Khan, F.; Kim, S.; McGee, R.; Li, Z.; Hu, Z.; Lee, J.; Thundat, T. Direct-current triboelectricity generation by a sliding Schottky nanocontact on MoS2 multilayers. *Nat. Nanotechnol.* **2018**, *13* (2), 112−116.
(8) Yang, R.; Benner, M.; Guo, Z.; Zhou, C.; Liu, J. High-Performance Flexible Schottky DC Generator via Metal/Conducting Polymer Sliding Contacts. *Adv. Funct. Mater.* **2021**, *31* (43), 2103132.
(9) Zheng, M.; Lin, S.; Xu, L.; Zhu, L.; Wang, Z. L. Scanning Probing of the Tribovoltaic Effect at the Sliding Interface of Two Semiconductors. *Adv. Mater.* **2020**, *32* (21), 2000928.
(10) Zhang, Z.; Jiang, D.; Zhao, J.; Liu, G.; Bu, T.; Zhang, C.; Wang, Z. L. Tribovoltaic Effect on Metal−Semiconductor Interface for Direct-Current Low-Impedance Triboelectric Nanogenerators. *Adv. Energy Mater.* **2020**, *10* (9), 1903713.
(11) Lin, S.; Chen, X.; Wang, Z. L. The tribovoltaic effect and electron transfer at a liquid-semiconductor interface. *Nano Energy* **2020**, *76*, 105070.
(12) Liu, J.; Cheikh, M. I.; Bao, R.; Peng, H.; Liu, F.; Li, Z.; Jiang, K.; Chen, J.; Thundat, T. Tribo-Tunneling DC Generator with Carbon Aerogel/Silicon Multi-Nanocontacts. *Adv. Electron. Mater.* **2019**, *5* (12), 1900464.
(13) Wang, Z. L. From contact electrification to triboelectric nanogenerators. *Rep. Prog. Phys.* **2021**, *84* (9), 096502.
(14) Liu, G.; Liu, J.; Dou, W. Non-adiabatic quantum dynamics of tribovoltaic effects at sliding metal−semiconductor interfaces. *Nano Energy* **2022**, *96*, 107034.
(15) Liu, J.; Liu, F.; Bao, R.; Jiang, K.; Khan, F.; Li, Z.; Peng, H.; Chen, J.; Alodhayb, A.; Thundat, T. Scaled-up Direct-Current Generation in MoS_2 Multilayer-Based Moving Heterojunctions. *ACS Appl. Mater. Interfaces* **2019**, *11* (38), 35404−35409.
(16) Benner, M.; Yang, R.; Lin, L.; Liu, M.; Li, H.; Liu, J. Mechanism of In-Plane and Out-of-Plane Tribovoltaic Direct-Current Transport with a Metal/Oxide/Metal Dynamic Heterojunction. *ACS Appl. Mater. Interfaces* **2022**, *14* (2), 2968−2978.
(17) Zhou, Y. S.; Wang, S.; Yang, Y.; Zhu, G.; Niu, S.; Lin, Z.-H.; Liu, Y.; Wang, Z. L. Manipulating Nanoscale Contact Electrification by an Applied Electric Field. *Nano Lett.* **2014**, *14* (3), 1567−1572.
(18) Lin, S.; Lu, Y.; Feng, S.; Hao, Z.; Yan, Y. A High Current Density Direct-Current Generator Based on a Moving van der Waals Schottky Diode. *Adv. Mater.* **2019**, *31* (7), 1804398.
(19) Lu, Y.; Feng, S.; Shen, R.; Xu, Y.; Hao, Z.; Yan, Y.; Zheng, H.; Yu, X.; Gao, Q.; Zhang, P.; Lin, S. Tunable Dynamic Black Phosphorus/Insulator/Si Heterojunction Direct-Current Generator Based on the Hot Electron Transport. *Research* **2019**, *2019*, 5832382.
(20) Lu, Y.; Hao, Z.; Feng, S.; Shen, R.; Yan, Y.; Lin, S. Direct-Current Generator Based on Dynamic PN Junctions with the Designed Voltage Output. *iScience* **2019**, *22*, 58−69.
(21) Liu, J.; Miao, M.; Jiang, K.; Khan, F.; Goswami, A.; McGee, R.; Li, Z.; Nguyen, L.; Hu, Z.; Lee, J.; Cadien, K.; Thundat, T. Sustained electron tunneling at unbiased metal-insulator-semiconductor tribo-electric contacts. *Nano Energy* **2018**, *48*, 320−326.
(22) Peljo, P.; Manzanares, J. A.; Girault, H. H. Contact Potentials, Fermi Level Equilibration, and Surface Charging. *Langmuir* **2016**, *32* (23), 5765−5775.
(23) Kaponig, M.; Mölleken, A.; Nienhaus, H.; Möller, R. Dynamics of contact electrification. *Sci. Adv.* **2021**, *7* (22), No. eabg7595.
(24) Liu, J.; Jiang, K.; Nguyen, L.; Li, Z.; Thundat, T. Interfacial friction-induced electronic excitation mechanism for tribo-tunneling current generation. *Mater. Horiz.* **2019**, *6* (5), 1020−1026.
(25) Imada, M.; Fujimori, A.; Tokura, Y. Metal-insulator transitions. *Rev. Mod. Phys.* **1998**, *70* (4), 1039−1263.
(26) Tselev, A.; Luk'yanchuk, I. A.; Ivanov, I. N.; Budai, J. D.; Tischler, J. Z.; Strelcov, E.; Kolmakov, A.; Kalinin, S. V. Symmetry Relationship and Strain-Induced Transitions between Insulating M1 and M2 and Metallic R phases of Vanadium Dioxide. *Nano Lett.* **2010**, *10* (11), 4409−4416.
(27) Wentzcovitch, R. M.; Schulz, W. W.; Allen, P. B. VO_2: Peierls or Mott-Hubbard? A view from band theory. *Phys. Rev. Lett.* **1994**, *72* (21), 3389−3392.
(28) Pouget, J. P.; Launois, H.; Rice, T. M.; Dernier, P.; Gossard, A.; Villeneuve, G.; Hagenmuller, P. Dimerization of a linear Heisenberg chain in the insulating phases of $V_{1-x}Cr_xO_2$. *Phys. Rev. B* **1974**, *10* (5), 1801−1815.
(29) Jördens, R.; Strohmaier, N.; Günter, K.; Moritz, H.; Esslinger, T. A Mott insulator of fermionic atoms in an optical lattice. *Nature* **2008**, *455* (7210), 204−207.
(30) Cyrot, M. Theory of mott transition: Applications to transition metal oxides. *J. Phys. (Paris)* **1972**, *33* (1), 125−134.
(31) Morin, F. J. Oxides Which Show a Metal-to-Insulator Transition at the Neel Temperature. *Phys. Rev. Lett.* **1959**, *3* (1), 34−36.
(32) Singamaneni, S. R.; Prater, J. T.; Narayan, J. Multifunctional epitaxial systems on silicon substrates. *Appl. Phys. Rev.* **2016**, *3* (3), 031301.
(33) Jian, J.; Wang, X.; Misra, S.; Sun, X.; Qi, Z.; Gao, X.; Sun, J.; Donohue, A.; Lin, D. G.; Pol, V.; Youngblood, J.; Wang, H.; Li, L.; Huang, J.; Wang, H. Broad Range Tuning of Phase Transition Property in VO_2 Through Metal-Ceramic Nanocomposite Design. *Adv. Funct. Mater.* **2019**, *29* (36), 1903690.
(34) He, Z.; Jian, J.; Misra, S.; Gao, X.; Wang, X.; Qi, Z.; Yang, B.; Zhang, D.; Zhang, X.; Wang, H. Bidirectional tuning of phase transition properties in Pt: VO_2 nanocomposite thin films. *Nanoscale* **2020**, *12* (34), 17886−17894.
(35) Sohn, A.; Kim, H.; Kim, D.-W.; Ko, C.; Ramanathan, S.; Park, J.; Seo, G.; Kim, B.-J.; Shin, J.-H.; Kim, H.-T. Evolution of local work function in epitaxial VO2 thin films spanning the metal-insulator transition. *Appl. Phys. Lett.* **2012**, *101* (19), 191605.
(36) Shao, H.; Fang, J.; Wang, H.; Dai, L.; Lin, T. Polymer−Metal Schottky Contact with Direct-Current Outputs. *Adv. Mater.* **2016**, *28* (7), 1461−1466.
(37) Zylbersztejn, A.; Mott, N. F. Metal-insulator transition in vanadium dioxide. *Phys. Rev. B* **1975**, *11* (11), 4383−4395.
(38) Brito, W. H.; Aguiar, M. C. O.; Haule, K.; Kotliar, G. Metal-Insulator Transition in VO_2: A DFT+DMFT Perspective. *Phys. Rev. Lett.* **2016**, *117* (5), 056402.
(39) Jager, M. F.; Ott, C.; Kraus, P. M.; Kaplan, C. J.; Pouse, W.; Marvel, R. E.; Haglund, R. F.; Neumark, D. M.; Leone, S. R. Tracking the insulator-to-metal phase transition in VO_2 with few-femtosecond extreme UV transient absorption spectroscopy. *Proc. Natl. Acad. Sci. U. S. A.* **2017**, *114* (36), 9558−9563.
(40) O'Callahan, B. T.; Jones, A. C.; Hyung Park, J.; Cobden, D. H.; Atkin, J. M.; Raschke, M. B. Inhomogeneity of the ultrafast insulator-to-metal transition dynamics of VO_2. *Nat. Commun.* **2015**, *6* (1), 6849.
(41) Lysenko, S.; Rua, A. J.; Vikhnin, V.; Jimenez, J.; Fernandez, F.; Liu, H. Light-induced ultrafast phase transitions in VO_2 thin film. *Appl. Surf. Sci.* **2006**, *252* (15), 5512−5515.
(42) Lysenko, S.; Rúa, A.; Vikhnin, V.; Fernández, F.; Liu, H. Insulator-to-metal phase transition and recovery processes in VO_2 thin films after femtosecond laser excitation. *Phys. Rev. B* **2007**, *76* (3), 035104.
(43) Crunteanu, A.; Givernaud, J.; Leroy, J.; Mardivirin, D.; Champeaux, C.; Orlianges, J.-C.; Catherinot, A.; Blondy, P. Voltage-

https://doi.org/10.1021/acs.nanolett.2c03481
Nano Lett. 2022, 22, 9084−9091

and current-activated metal−insulator transition in VO_2-based electrical switches: a lifetime operation analysis. *Sci. Technol. Adv. Mater.* **2010**, *11* (6), 065002.
(44) Zohar, A.; Kulbak, M.; Levine, I.; Hodes, G.; Kahn, A.; Cahen, D. What Limits the Open-Circuit Voltage of Bromide Perovskite-Based Solar Cells? *ACS Energy Lett.* **2019**, *4* (1), 1−7.
(45) Liao, Z.-M.; Liu, K.-J.; Zhang, J.-M.; Xu, J.; Yu, D.-P. Effect of surface states on electron transport in individual ZnO nanowires. *Phys. Lett. A* **2007**, *367* (3), 207−210.
(46) Liu, L.; Kong, L.; Li, Q.; He, C.; Ren, L.; Tao, Q.; Yang, X.; Lin, J.; Zhao, B.; Li, Z.; Chen, Y.; Li, W.; Song, W.; Lu, Z.; Li, G.; Li, S.; Duan, X.; Pan, A.; Liao, L.; Liu, Y. Transferred van der Waals metal electrodes for sub-1-nm MoS_2 vertical transistors. *Nat. Electron.* **2021**, *4* (5), 342−347.
(47) Unsworth, J.; Jin, Z.; Lunn, B. A.; Innis, P. C. Development and characterisation of polypyrrole/metal junctions for electronic applications. *Polym. Int.* **1991**, *26* (4), 245−249.
(48) Abthagir, P. S.; Saraswathi, R. Junction properties of metal/polypyrrole Schottky barriers. *J. Appl. Polym.* **2001**, *81* (9), 2127−2135.
(49) Potje-Kamloth, K. Semiconductor Junction Gas Sensors. *Chem. Rev.* **2008**, *108* (2), 367−399.

https://doi.org/10.1021/acs.nanolett.2c03481
Nano Lett. 2022, 22, 9084−9091